Paper 110
Assessment of CFD Methods against Experimental Flow Measurements for Helicopter Flows

B. Zhong[*1], D. Drikakis[*2], A. Antoniadis[*3], G. Barakos[4], M. Biava[5], A. Brocklehurst[6], O. Boelens[7], M. Dietz[8], M. Embacher[9], W.Khier[10], T.Renaud[11], R. Steijl[12], L. Vigevano[13]

---

[*] Corresponding authors

[1] Department of Aerospace Sciences, Cranfield University, Cranfield, Bedfordshire MK43 0AL, UK, email: b.zhong@cranfield.ac.uk

[2] Cranfield University, email: d.drikakis@cranfield.ac.uk

[3] Cranfield University, email: a.f.antoniadis@cranfield.ac.uk

[4] University of Liverpool

[5] Politecnico de Milano

[6] AgustaWestland

[7] Nationaal Lucht - en Ruimtevaartlaboratorium

[8] Eurocopter Deutschland GmbH

[9] Institut für Aerodynamik und Gasdynamik der Universität Stuttgart

[10] Deutsches Zentrum für Luft- und Raumfahrt e.V.

[11] Office National d'Etudes et de Recherches Aérospatiale

[12] University of Liverpool

[13] Politecnico di Milano

Abstract

A novel computational and experimental aerodynamic database for helicopter flows has been developed. The establishment of a validation tool for the design and development of CFD methods was the primary objective. Several flow simulations and wind tunnel tests have been carried out in a recent European research project; GoAHEAD (Generation of Advanced Helicopter Experimental Aerodynamic Database for CFD code validation). The wind-tunnel measurements have been performed at DNW wind tunnel. According to the post-test specifications, calculations for six test cases have been conducted by nine GOAHEAD project partners: three isolated fuselage tests, a low speed pitch-up case, a cruise and high speed tail shake case and highly loaded dynamic stall case. In this paper, results using different CFD methods are assessed and compared with the experimental measurements. The results include the cross-sectional steady and unsteady pressures on the fuselage and rotors, velocity contour plots and corresponding PIV flow visualisations.

Nomenclature

a_∞	Free-stream speed of sound [m/s]
C_p	Pressure coefficient $= 2(p-p_\infty)/(\rho_\infty U_\infty^2)$
$C_p M^2$	Blade sectional pressure coefficient $= 2(p-p_\infty)/(\rho u_i^2)(u_i/a_\infty)^2$
r	Radial position along rotor blade [m]
R	Rotor radius [m]
M_{WT}	Wind tunnel Mach number
M_{tipTR}	Tail rotor tip Mach number
M_{tipMR}	Rotor tip Mach number
p	Pressure [N/m^2]
p_∞	Free-stream pressure [N/m^2]
U_∞	Free-stream velocity [m/s]
θ_F	Fuselage pitch attitude [^{o}]
ρ_∞	Free-stream density [kg/m^3]
ψ	Main rotor azimuth angle: zero with one of the blades parallel to the positive x axis. Main rotor is rotating clockwise viewed from above [^{o}]

Abbreviations

CFD	Computational Fluid Dynamics
CUN	Cranfield University
DG	Discontinuous Galerkin
DLR	Deutsches Zentrum für Luft- und Raumfahrt e.V. DLR
DNW	German-Dutch Wind Tunnels
ECD	Eurocopter Deutschland GmbH
ECF	Eurocopter S.A.S.
elsA	Ensemble logiciel de simulation en aérodynamique
FOR	Foundation for Research and Technology FORTH
GOAHEAD	Generation Of Advanced Helicopter Experimental Aerodynamic Database for CFD code validation
HLLC	Harten-Lax-van Leer-Contact solver
HMB	Helicopter Multi-Block
HOST	Helicopter Overall Simulation Tool
IAG	Institut für Aerodynamik und Gasdynamik der Universität Stuttgart
ILES	Implicit Large Eddy Simulation
MTMG	Multi-time multi-grid
MUSCL	Monotone Upstream-centered Schemes for Conservation Laws
NLR	Nationaal Lucht- en Ruimtevaartlaboratorium NLR
ONE	Office National d'Etudes et de Recherches Aérospatiale ONERA
PIV	Particle Image Velocimetry
POM	Politecnico di Milano
ROSITA	Rotorcraft Software Italy
SME	Small-medium Enterprise
SST	Shear Stress Transport
ULI	University of Liverpool
URANS	Unsteady Reynolds Average Navier Stokes equations
WENO	Weighted-Essential Non Oscillatory schemes
WHL	Westland Helicopters Ltd

I. Introduction

CFD solvers play a crucial role in the modern design process of many aeronautic applications. One of the main shortcomings of European helicopter design process is the industrial necessary requirement of detailed experimental database for the validation of CFD algorithms. This basic requirement initiated the GOAHEAD project in 2005 which included partners from five national research centres, five universities, four helicopter manufacturers and one SME. The nine partners who carried out the post test computations are Walid Khier, Deutsches Zentrum für Luft- und Raumfahrt e.V. DLR (DLR); Markus Dietz, Eurocopter Deutschland GmbH (ECD); Okko Boelens, Nationaal Lucht- en Ruimtevaartlaboratorium NLR (NLR); Thomas Renaud, Office National d'Etudes et de Recherches Aérospatiale ONERA (ONE); Alan Brocklehurst, AgustaWestland (WHL); Bowen Zhong and Dimitris Drikakis, Cranfield University (CUN), Martin Embacher, Institut für Aerodynamik und Gasdynamik der Universität Stuttgart (IAG); M. Biava and Luigi Vigevano, Politecnico di Milano (POM); Rene Steijl and George Barakos, University of Liverpool (ULI).[1] The project is partially funded by the European Union under the Integrating and strengthening the European Research Area Programme of the 6th Framework, Contract Nr. 5160714.

Helicopter airflow is dominated by complex aerodynamics and flow interactions. The main rotor blades and the tail rotor stabilizer amplify the airflow turbulence intensity. In order to efficiently capture these interactions, state-of-the-art CFD methods were employed on a helicopter model.

II. CFD Methods

Four different types of spatial computational grids were generated for the fuselage, rotor head, main rotor blades, tail rotor and wind tunnel walls; the chimera grid by DLR, the sliding-grid approach by ULI, the sliding-disk approach by NLR and an unstructured grid approach by Foundation for Research and Technology (FORTH) [13].

Several CFD solvers were employed in the GOAHEAD project: the elsA solver developed by Eurocopter S.A.S. and ONE [8]. The FLOWer code developed by DLR[7], the HMB solver from WHL

and ULI [9], the Rosita solver used by Agusta S.P.A. and POM [10]. A Discontinuous Galerkin MTMG approach combined with ENSOLV from NLR and FORTH/IACM [14,15].

Several high-resolution schemes for turbulent flow simulations have been implemented in the FLOWer solver by CUN [11] including MUSCL, the 3rd order WENO schemes, and the HLLC approximate Riemann solver in the framework of a URANS and ILES approach. A detailed overview of the CFD methods used for the GOAHEAD project can be found in [16].

III.   Preliminary Computations – Blind-Test phase

A series of numerical computations have been conducted by the GOAHEAD partners before and after the experimental activities in the DNW wind tunnel facilities. The blind-test computations have been performed during the first two years of the GOAHEAD project. Computations have been carried out for six test cases; three isolated fuselage (TC1a, TC1b, TC1c), a low speed pitch-up case (TC2) and the cruise and tail shake cases (TC3-4). The blind-test results provided a first overview of the aerodynamic effects to be expected by the wind tunnel measurements [6]. A comparison has been conducted for the blind test phase between the computational and the experimental results [3].

IV.   Experimental Activities

The experimental activities encompass airflow measurements from steady and unsteady pressure sensors, Particle Image Velocimetry (PIV), hot films, infrared images techniques and surface flow visualization with tufts. Figure 1 illustrates the steady and unsteady sensors position on the fuselage. Figure 2 indicates the unsteady pressure sensor locations. The planes used in the simulation activities are selected in such a way to be in agreement with the position of the pressure sensors and PIV planes (Figure 3) which are used in the wind tunnel measurements. UGL developed a post-processor used for extracting the measured data from the GOAHEAD experimental raw database. [23]

V.   Final Computations – Post-Test phase

After completing the assessment and comparison of the blind-test phase with the experimental results, modifications were made in the final computation work packages for the post-test calculation phase. The post-test simulations utilized a more detailed model, closer resembling that used for the wind tunnel test. Also, the initial and flight conditions were modified

according to the wind tunnel free-stream conditions. A total of seven test cases were simulated: the TC1a, TC1b, TC1c, TC2, TC3-4 tests used in the preliminary computations (see Section III) and a highly loaded dynamic stall case (TC5). Table 2 details the complete flow parameters of each case.
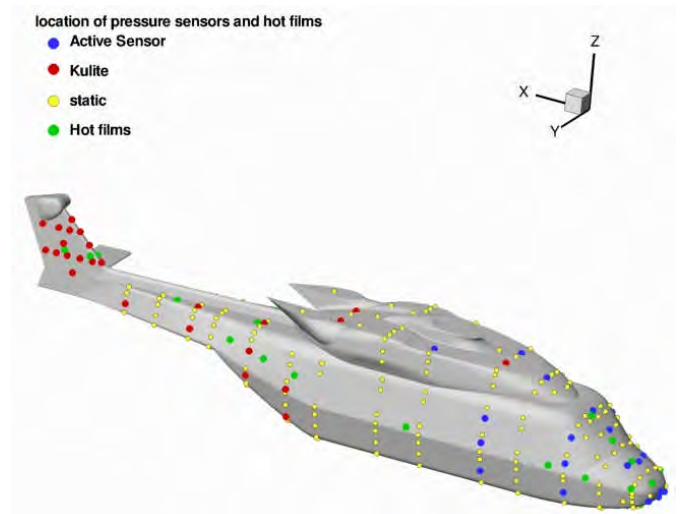

Figure 1: Steady and hot film sensor positions

Partner	Flow Solver	1a	1b	1c	2	3&4	5
CUN	FLOWer HLLC,WENO		√	√			
DLR	FLOWer						√
ECD	FLOWer	√	√				√
IAG	FLOWer				√		
NLR	ENSOLV		√			√	
POM	ROSITA					√	
ULI	HMB		√			√	√
WHL	HMB					√	

Table 1: Test cases of the post-test computations of each GOAHEAD partner and the flow solver employed

Test Case	TC1a	TC1b	TC1c
M_{WT}	0.059	0.204	0.258
θ_F	+4.8^o	-2.0^o	-1.0^o

Test Case	TC2	TC3&4	TC5
M_{WT}	0.059	0.204	0.194
θ_F	+1.88^o	-2.5^o	+1.0^o
M_{tipMR}	0.617	0.617	0.617
M_{tipTR}	0.563	0.563	0.563

Table 2: Test case and flight parameters for post-test computations
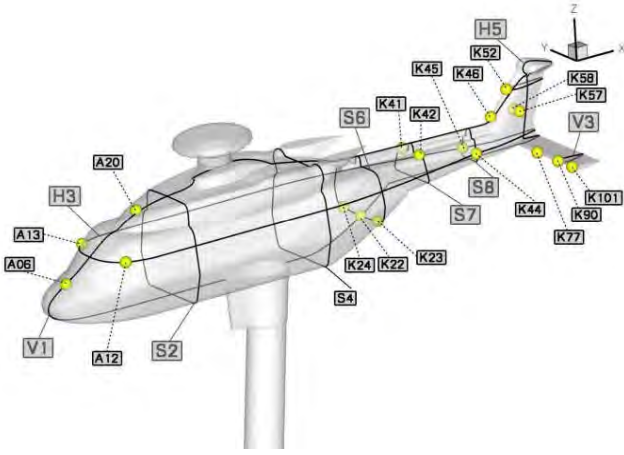
Figure 2: Sectional planes and unsteady sensor positions
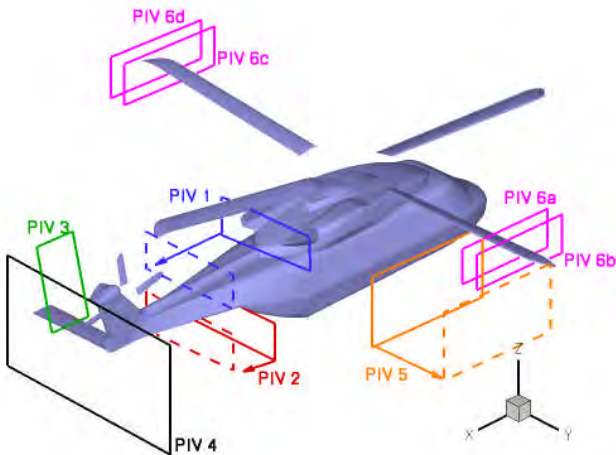

Figure 3: PIV measurement positions

VI.   Isolated fuselage cases - TC1(a,b,c)

Three cases have been simulated for the isolated helicopter fuselage by CUN, ECD, NLR and ULI.

Wind-tunnel measurements have been performed to provide reference data for the fuselage. Steady state solution was simulated neglecting the rotor blades but including the rotor head. A low mach-number preconditioning treatment was employed for all numerical computations. Case TC1b will form the focus in this paper for the isolated fuselage cases.

Figure 4 in Appendix A shows a comparison of the average pressure coefficients for the unsteady sensors at 17 positions on the helicopter fuselage. The CFD results are in good agreement with those from the experiment. Sensor K90 located on the tail stabilizer proved to be unstable, mainly due to the occurrence of sharp pressure variations at this location. Figure 5 illustrates the computed sectional surface pressure coefficient C_p at sections V1 and V3. The experimental measurements are in acceptable agreement. Minor overestimations of the pressure

coefficient can be observed at the main rotor head and tail section. Moreover the field view of all four computational results for the plane intersecting the fuselage at section X=0.970 (Figure 6) and with the PIV1 experimental data demonstrates the existence of four main vortices above the fuselage. CUN, ECD and ULI have almost symmetric flow fields, while NLR produced a larger vortex on the left side. The vortices undoubtedly originate from the engine's double exhausts located between plane S4 and S6. Overall for the isolated fuselage test case the computational results are satisfactory and in good agreement with the measurements.

VII.   Low speed pitch up case – TC2

Pitch-up occurs when the main rotor wake impinges and interacts with the horizontal stabilizer tail flow during transition from hover to low or medium speeds. ECD computed the flight conditions (Table 2) and the fuselage angles using the aeromechanical code HOST [17]. Computations for the low speed pitch-up test case were performed by IAG. A weak coupling of the flow solver FLOWer with the HOST code [7] has been accomplished by IAG.

Figure 7 in Appendix A is a representation of the sectional surface pressure coefficient C_p at sections S7 (a) and H5 (b) for this test case. The lines correspond to the computational data and the scatter symbols to the experimental measurements for main rotor azimuth. Data is shown for azimuth angles $\psi=0°$, $\psi=30°$ and $\psi=60°$ separately for each blade. Several discrepancies are clearly observed on the S7 plane, the location is dominated by strong turbulence vortices mainly due to the position under the main rotor blades and behind the main rotor head and the exhaust system. On the plane H5 the agreement is much more reasonable. One can clearly observe the interaction effect of the main rotor on the vertical tail.

Figure 8 illustrates surface pressure coefficient of the helicopter fuselage for three azimuth intervals ($\psi=0°$, $\psi=30°$ and $\psi=60°$). Calculation and experiment are in disagreement for certain locations, near the front nose right side and horizontal stabilizer. Variations of the computational contour plots with the azimuths clearly establish an unsteady flow regime.

VIII.   Cruise and high speed, tail-shake case TC3-4

In interactional helicopter aerodynamics the tail-shake is a repeating phenomenon that occurs at high speeds as a consequence of the interaction of the main rotor blade's wake with the tail boom and the vertical tail [19]. This aerodynamic interaction originates from several design characteristics such as the main rotor

4

hub, engine intakes, exhaust pipes, cowling shapes and the proximity of the rotor with the fuselage. As a corollary of this turbulent reciprocal effect, excessive low frequency vibration has been confirmed in the vicinity of the flight crew station [19].

The pitch attitude was set to -2.5^o by rotating the model forward until tail-shake was confronted. By employing the aeromechanical code HOST [17] developed by EC SAS and using the pitch attitude angle as well as the flight parameters of Table 2, the blade trimming angles were calculated. Computations have been performed by four partners NLR, POM, ULI and WHL. NLR simulated both main and tail rotor, including a sliding grid capability with spline interpolation as well as an aeroelastic blade deformation algorithm [15]. DLR used similar trimming approach with IAG for the TC2 case and integrated an elastic blade deformation model also used by POM. POM employed a Roe-Turkel preconditioning algorithm along with the ROSITA solver [20]. ULI used the blade control angle obtained by ECD.

Velocity magnitude contours and stream lines are used for the comparison and flow visualization. Figure 9 (a) shows the computed solution of POM and NLR for the sectional plane at x=0.970 for 30° azimuth main rotor angle. Both solutions confirm the presence of two main asymmetric counter-rotating vortices with the PIV captured data. The unsteadiness of this case is clearly exemplified; secondary vortices are generated near the centre symmetric tip and fuselage surface. The discontinuity of the streamlines and the sudden variation of the velocity at approximately Z=0.65 of the computed solutions demonstrate the effect of the rotating main rotor blades. As in the steady state isolated fuselage case for the same sectional plane (Figure 6), the creation of the vortical structures is initiated by the exhaust system pipes. The stream-lines of sectional plane, x=1.463 underneath the fuselage at approximately section S4 (azimuth 0°) shows two vortices, also predicted by the PIV data.

Pressure sensor data (C$_p$) for the cruise high speed case are presented in Figure 10. Computational results are available for three partners (NLR, POM and ULI) for comparison with the experimental data from the unsteady sensors at 18 locations on the helicopter fuselage for one rotor revolution. The wave shape of the figure obviously demonstrates the incorporation of the main rotor in the model. Overall NLR and ULI are in very good agreement with the measurements, POM computations introduce pressure overestimations. Sensor K24 located at the rear door seems to be malfunctioning with an average difference of approximately 0.2 from the computed solutions. As in the isolated fuselage case (Figure 4), the largest

discrepancies are detected on the horizontal stabilizer sensors K77 and K90. The unsteady sensors indicate an irregular behaviour attributed to flow separation or to the submission of the horizontal stabilizer to wake flow or combination of both [18]. Wake formation can be regarded as a reason of this misbehaviour due to flow interactions of the main rotor head fairing with the blade root region and the left engine exhaust. It has also been confirmed by the "Flow Separation Visualization" [21] that on the upper outboard surface of the stabilizer (K90) the turfs are relatively stationary where as on the lower suction surface they are in motion indicating that a flow separation could be occurring.

Blade sectional pressure coefficient (C$_p$M^2) of the main rotor at the radial position r/R=0.70 for one revolution with 30° intervals are presented in Figure 11. Four partners provided computational data: ULI, NLR, POM and WHL for the isolated main rotor. Calculations are in good agreement with the experiment, the apparent differences seen mainly at the front and rear of the disc, are generally consistent with expectations as determined by Barakos and Steijl [24]. The CFD solutions predict a transonic flow reduction at the blade tips, attributed to the parabolic swept back tip of the rotor blade.

IX. Highly loaded rotor, dynamic-stall case – TC5

Dynamic-stall in rotorcraft aerodynamics occurs at average to high horizontal flight speeds, where the local angle of attack of the blades and the potential change of inflow conditions are the primary cause of this unsteady phenomenon [22]. High local angles of attack on the retreating blade may induce the formation of a vortex, located on the leading edge of the blades. The detached flow will move downstream and stall conditions will appear affecting the local blade lift and the pitching moment. While the vortex travels from the leading to the trailing edge the pitching moment turns negative. The lift will increase but will drop suddenly after the flow separation, resulting in twisting of the rotor blade. The periodical stalled region over the rotor will generate high varying forces leading to vibration that might be destructive for the structure.

Three partners performed computations for the isolated rotor test case; ECD, DLR and ULI. ECD employed a refined blade grid and trimmed the rotor according to the actual wind tunnel trim state. ECD and DLR used the FLOWer solver [7] incorporating a weak coupling of the aeromechanical code HOST [17] for trimming the rotor and updating the aerodynamic loads. Also a fully turbulent model (Wilcox k-Ω) was employed, the physical time step was reduced to 0.5^o

azimuth to obtain better resolution. ULI used the HMB solver[9]. The trim state used for the post-test calculations presented in this work was based on the measured angles from the wind tunnel experiment and the Wilcox k-omega model was used with an azimuthal step of 0.25 degree.

Data of sectional blade pressure coefficient C_pM^2 at 30° azimuthal intervals are shown in Figures 12 and 13 for radial position r/R=0.50 and r/R=0.98. Disagreement between CFD and experiment is visible for r/R=0.50 at azimuth 180° and a sensor near the trailing edge was found to be defective. The results for r/R=0.98 are in acceptable agreement with a more extensive variation of C_pM^2. A shockwave is formed at azimuth $\psi=30°$ to $\psi=210°$, where the sudden drop of the pressure coefficient is noticeable for all computed solutions.

Dynamic stall phenomenon appears on the retreating side of the rotor, at the radial position r/R=0.98 between azimuth 270° and 360° where the blade pressure coefficient drops suddenly indicating presence of flow separation.

X.   Concluding remarks

This paper presents an assessment of several state-of-art CFD methods and experimental measurements of a complete helicopter flow for various flight configurations. The paper represents a small fraction of the post-processed data under the work-package of the GOAHEAD project. In most of the cases a reasonably good agreement is seen between computations and experimental results. The employed CFD tools demonstrated themselves capable to successfully predict the physical phenomena dominating a helicopter flow. Overall the entire GoAHEAD project provides a significant scientific and commercial advantage to the design and validation of CFD solvers.

XI.   Acknowledgements

References

[1] K. G. Pahlke, "The GOAHEAD Project", 33rd European Rotorcraft Forum, Russia, September 11th-13th, 2007.

[2] O. J. Boelens, "Post test phase data specification for deliverables D2.2.3", GOAHEAD/ WP2/ NLR / D2.2.3/ A, 2009.

[3] B. Zhong, A. Antoniadis, D. Drikakis, "A Comparison of Blind-Test Computations with Experimental Data", GOAHEAD/ WP4/CU/D4.3.1, 2009.

[4] A. Antoniadis, B. Zhong, D. Drikakis, "A Comparison of Post-Test Computations with Experimental Data", GOAHEAD/WP4/CU/D4.3.2, 2009.

[5] Deutsches Zentrum für Luft- und Raumfahrt e.V. DLR, "Generation of Advanced Helicopter Experimental Aerodynamic Database for CFD code validation – GOAHEAD – Contract Nr. 516074: Annex I – Description of Work", 2005.

[6] O.J. Boelens, G. Barakos, M. Biava, A. Brocklehurst, M. Costes, A. D'Alascio, M. Dietz, D. Drikakis, J. Ekaterinaris, I. Humby, W. Khier, B. Knutzen, J. Kok, F. LeChuiton, K. Pahlke, T. Renaud, T. Schwarz, R. Steijl, L. Sudre, H. van der Ven, L. Vigevano and B. Zhong, "The Blind-test activity of the GOAHEAD project", 2007.

[7] K. Becker, N. Kroll, C.C. Possow and F. Thiele, "The MEGAFLOW project", Aerospace Scie. Technol. 4, 2000, pp. 223-237

[8] M. Gazaix, A. Jolles and M. Lazareff, "The elsA object-oriented computational tool for industrial application", 23rd ICAS conference, Semptember 2002.

[9] R. Steijl, G. Barakos and K. Badcock, "A framework for CFD analysis of rotors in hover and forward flight", Int. J. for Num. Meth. In Fluids, vol. 51, 2006, pp. 819-847.

[10] M. Biava, J-C. Boniface and L. Vigevano, "Influence of wind-tunnel walls in helicopter aerodynamics predictions", 31st European Rotorcraft Forum, Florence, Italy 2005.

[11] D. Drikakis, "Advances in turbulent flow computations using high-resolution methods", Progress in Aerospace Sciences, Vol. 39, pages 405-422, 2003.

[12] R. Steijl and G. Barakos, "Sliding-Mesh Algorithm for CFD Analysis of Helicopter Rotor-Fuselage Aerodynamics", Conference on Aeromechanics, San Francisco , Ca, January 23-25, 2008.

[13] W. Khier, "Description of GOAHEAD CFD grids", GOAHEAD/WP2/DLR/D2.1.2/A, 2006.

[14] "ENFLOW: A computer code system for accurate simulation of three-dimensional flows", July 2007.

[15] H. Van der Ven and O.J. Boelens, "A framework for aeroelastic simulations of trimmed rotor systems in forward flight", 30th European Rotorcraft Forum, Marseille, France, 2004.

[16] T. Renaud, "Description of the CFD methods", GOAHEAD/WP2/ONERA/M2.1.2, 2006.

[17] B. Benoit, A.M.Dequin, K.Kamp, W. Von Gruenhagen, P.M. Basset and B. Gimonet, "HOST, a general helicopter simulation tool for Germany and France", In American Helicopter Society 56th Annual Forum, Virginia Beach, Virginia, USA, 2-4 May 2000. AHS.

[18] T. Renaud, "Improved methodologies for post-test computations", GOAHEAD/WP2/ONERA/D2.2.1.

[19] P.G. de Waard and M. Trouvé, "Tail shake vibration Objective comparison of aerodynamic configurations in a subjective environment", 55th American Helicopter Society Annual Forum, Montreal, Canada, 1999.

[20] E. Turkel, R. Radespiel and N. Kroll, "Assessment of Preconditioning Methods for Multidimensional Aerodynamics", Comp. and Fluids, 6, 613-634 (1997).

[21] M. Raffel, "Flow Separation Visualization", GOAHEAD/WP3/DLR/D3.8.4

[22] I. Humby, C. Castellin, B.G. van der Wall, K. Pahlke and T. Schwarz, "Definition of the experimental & CFD test matrix", GOAHEAD/WP1/EC/D1.1&2 D2.1.1/D.

[23] W. Sheng, "Data Post-Processor", GOAHEAD/WP4/UG/D4.1.4/A

[24] R. Steijl and G.N. Barakos, "A Computational Study of Helicopter Rotor Fuselage Aerodynamic Interactions", AIAA Journal, Vol.47, No 9, September 2009.

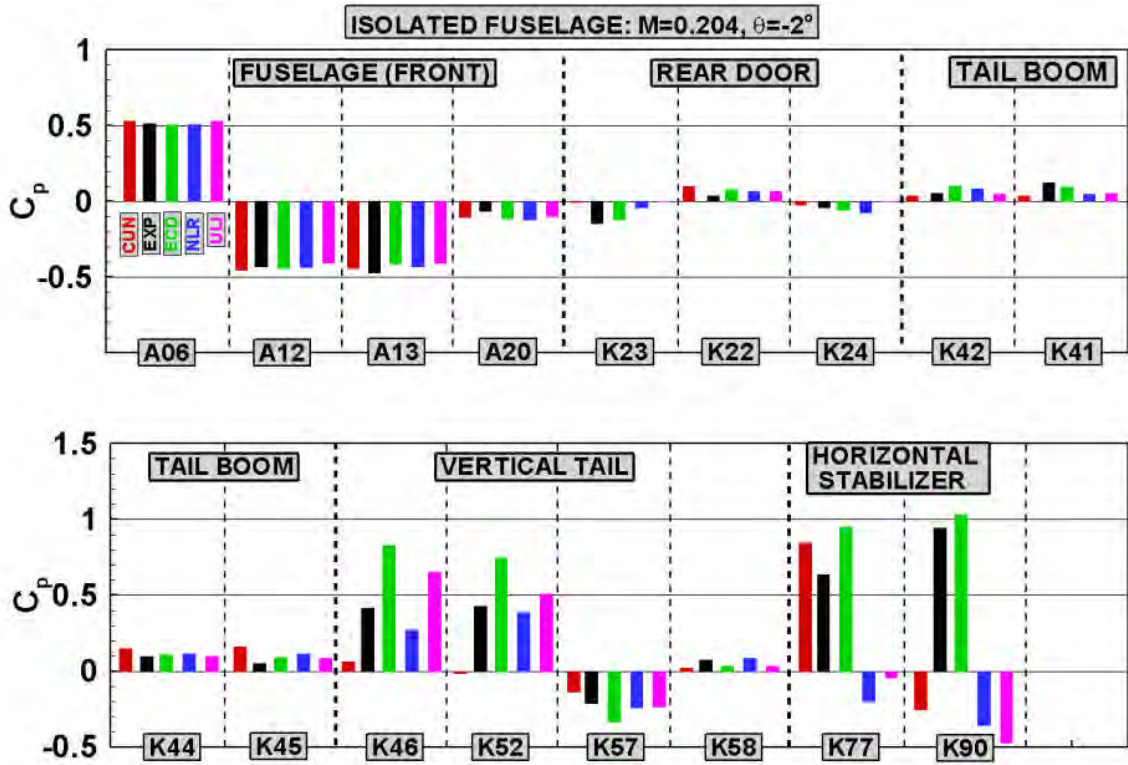## Appendix A

a. *Isolated Fuselage TC1b*

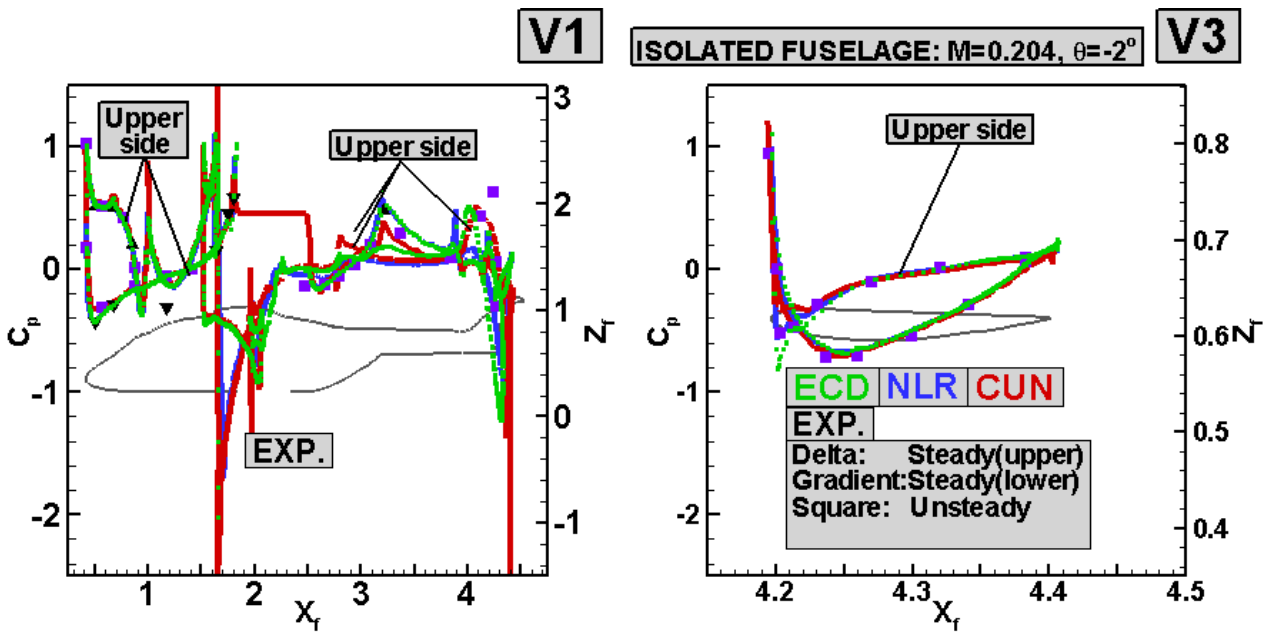**Figure 4: Pressure sensor data C$_p$ for TC1b**

Figure 5: Sectional surface pressure coefficient C$_p$ at section V1 and V3 for TC1b
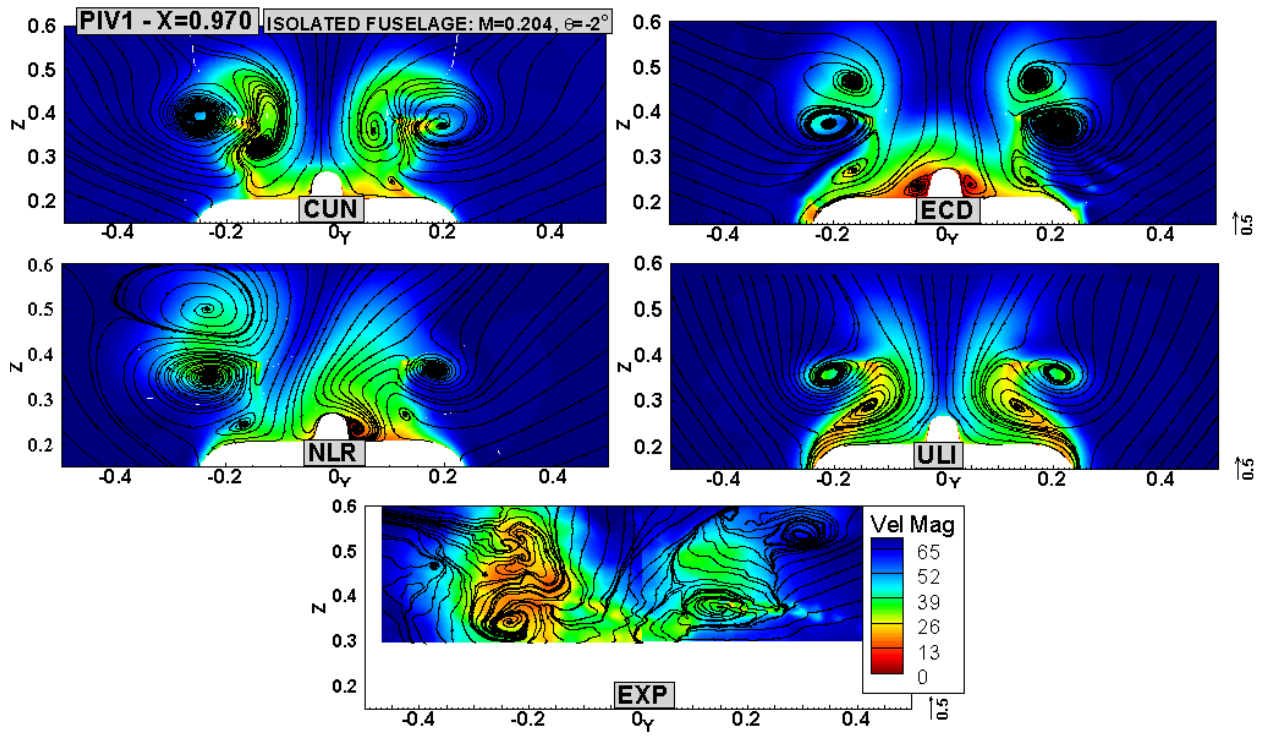
Figure 6: Velocity magnitude (m/s) and stream-traces for section X=0.970 and PIV1 – TC1b
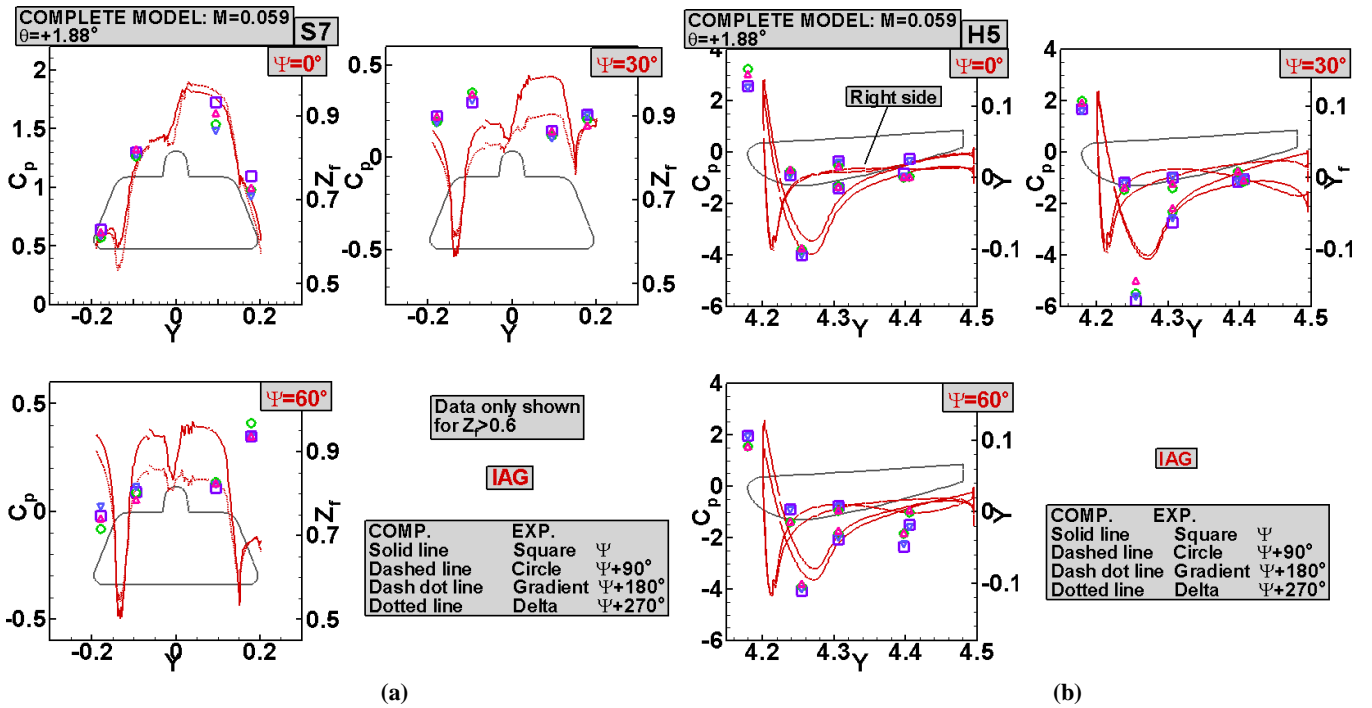
b. *Low Speed (Pitch-up) Case TC2*

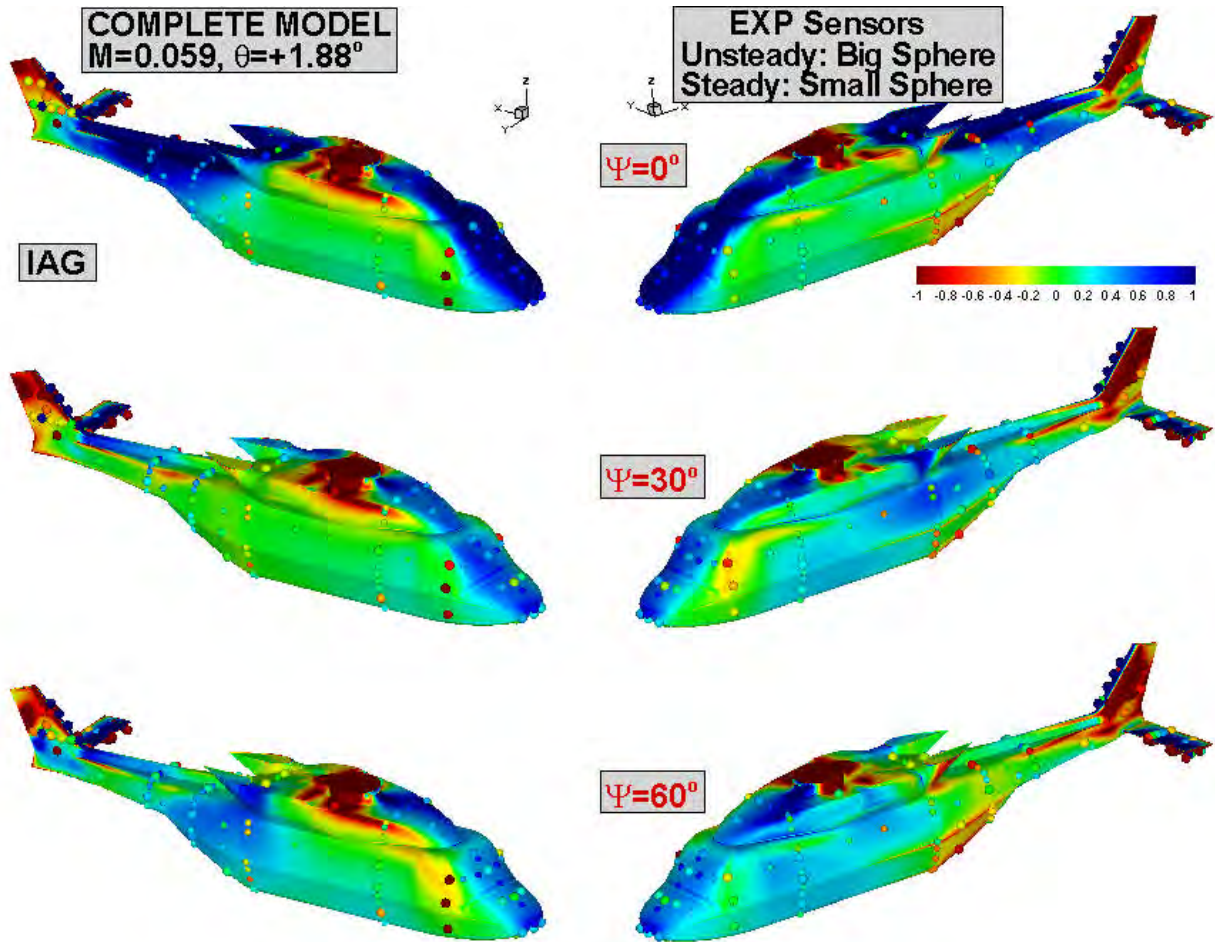**Figure 7: Sectional surface pressure coefficient C_p at section S7 (a) and H5 (b) for TC2**

Figure 8: Surface pressure coefficient C$_p$ at main rotor azimuth ψ=0°, 30 ^{o} and 60 ^{o} – TC2

c. *Cruise and High-Speed Tail-Shake Case TC3 – 4*
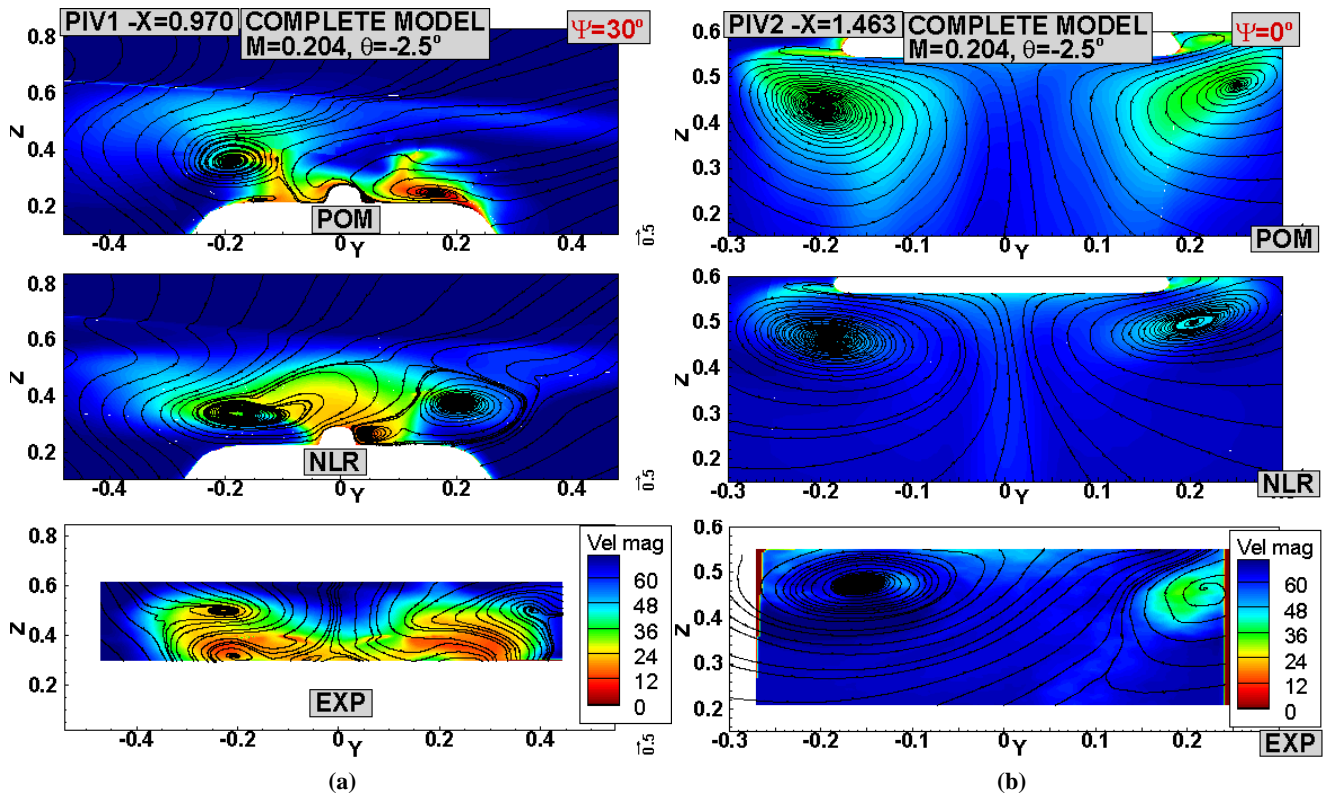
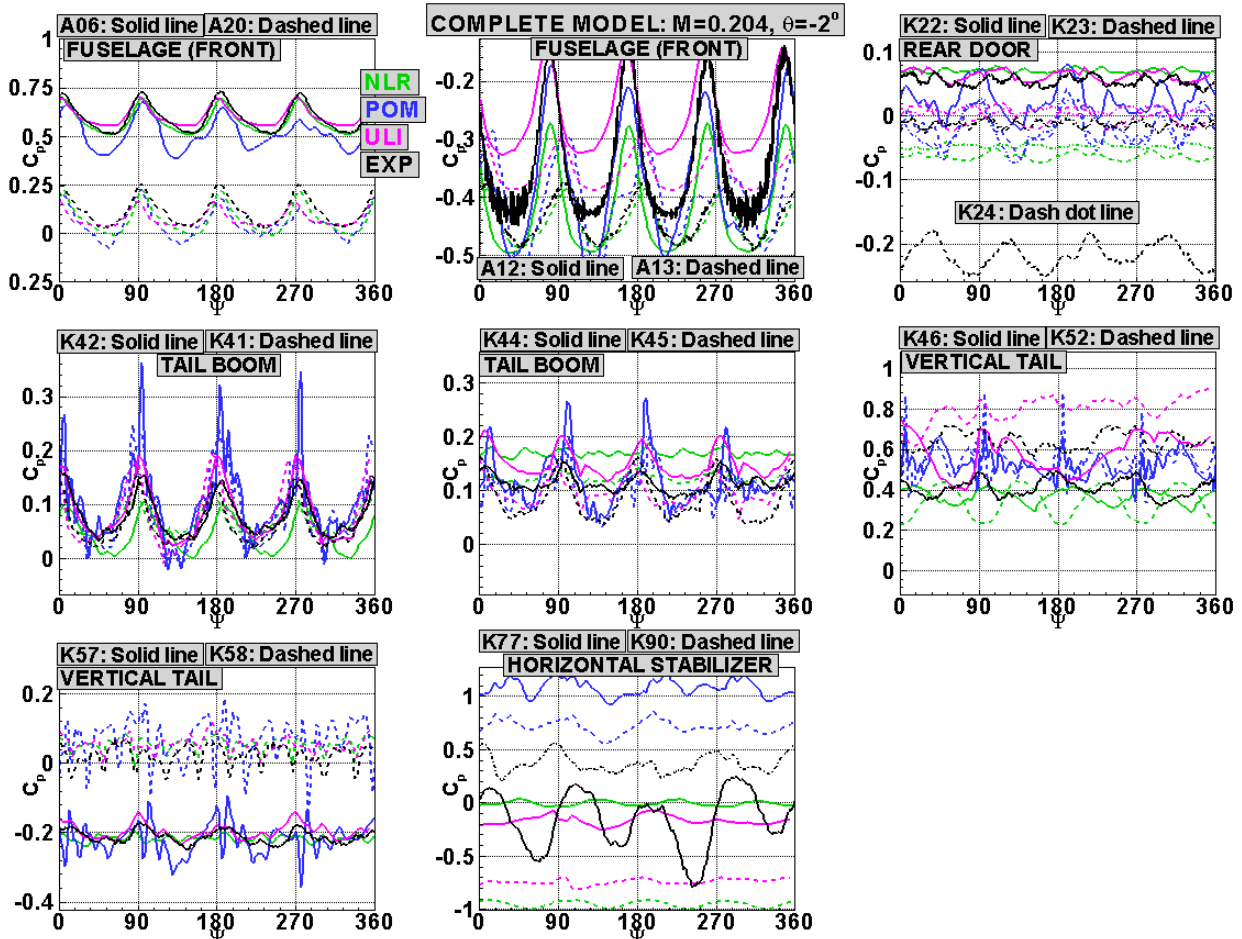**Figure 9: Velocity magnitude (m/s) and stream-traces for section X=0.970 (a) and X=1.436 (b) – TC3,4**

10

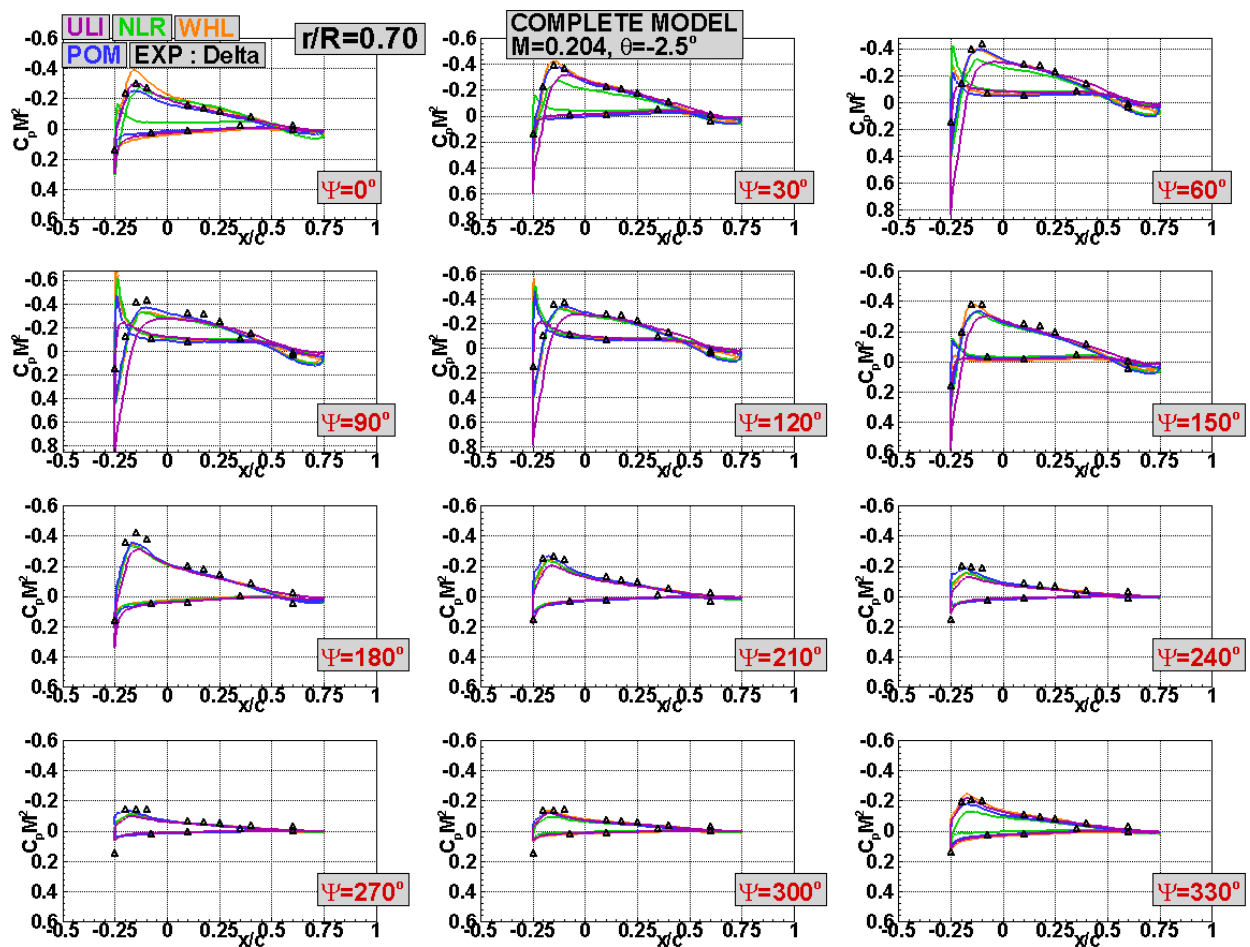**Figure 10: Pressure data C_p for TC2 at the sensor locations – TC3,4**

Figure 11: Sectional surface pressure data C_pM^2 for the main rotor at r/R=0.70 data is shown at 30° azimuthal intervals – TC3,4

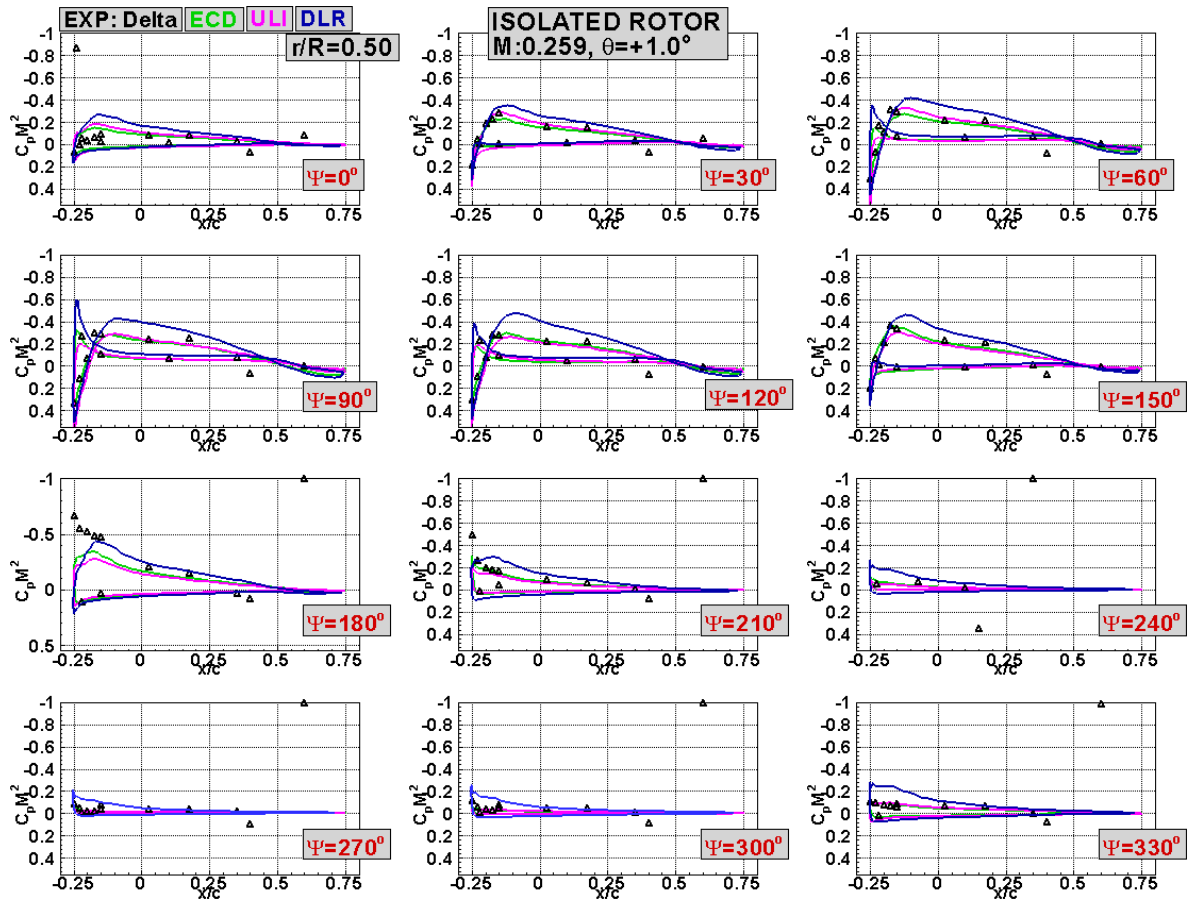## d. High Loaded Dynamic Stall Test Case TC5

Figure 12: Sectional surface pressure data C_pM^2 for the main rotor at r/R=0.50 data is shown at 30° azimuthal intervals - TC5
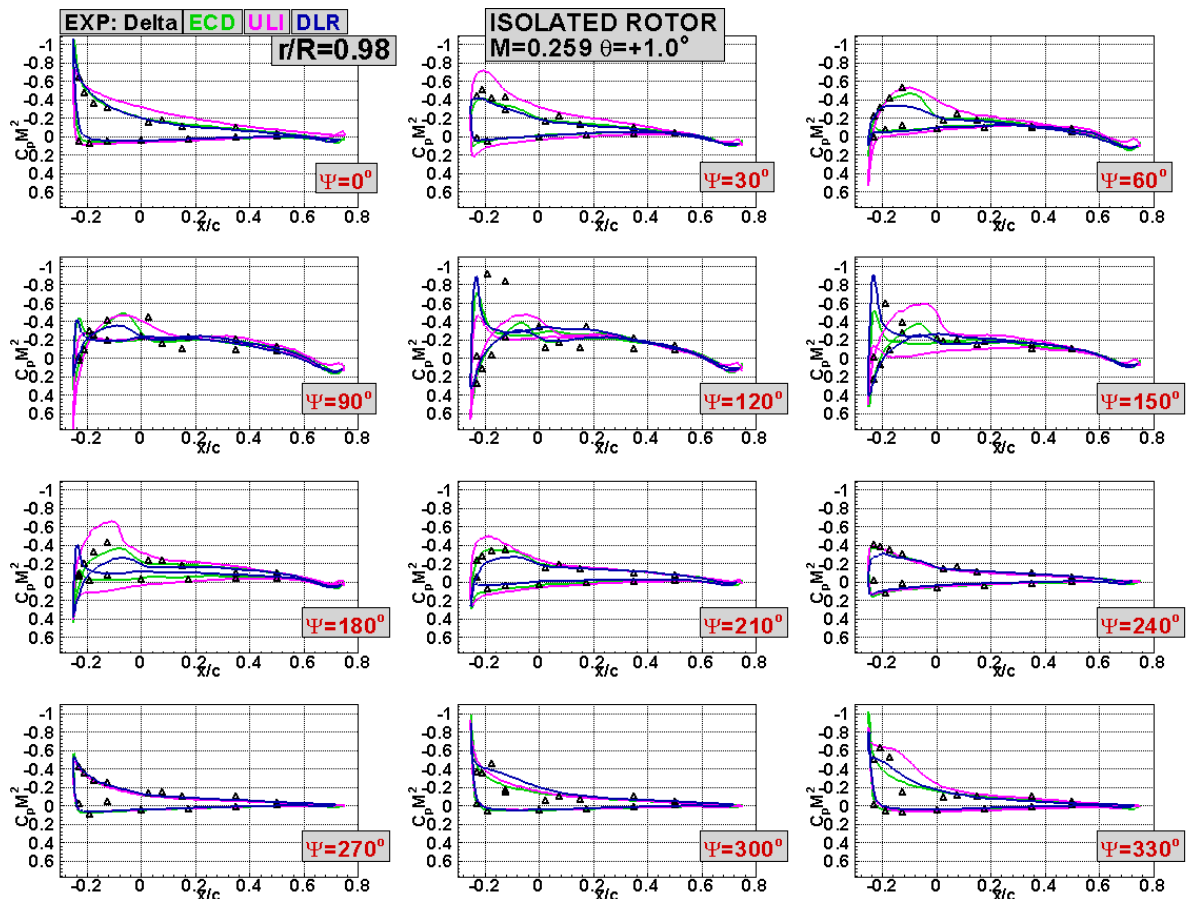

Figure 13: Sectional surface pressure data C_pM^2 for the main rotor at r/R=0.98 data is shown at 30° azimuthal intervals – TC5